# Using Discrete Multi-Physics for studying the dynamics of emboli in flexible venous valves

Ariane, M.; Vigolo, D.; Brill, A.; Nash, F. G.B.; Barigou, M.; Alexiadis, A.

*DOI:*
10.1016/j.compfluid.2018.01.037



*Document Version*
Peer reviewed version

*Citation for published version (Harvard):*
Ariane, M, Vigolo, D, Brill, A, Nash, FGB, Barigou, M & Alexiadis, A 2018, 'Using Discrete Multi-Physics for studying the dynamics of emboli in flexible venous valves', *Computers and Fluids*, vol. 166, pp. 57-63. https://doi.org/10.1016/j.compfluid.2018.01.037

# Using Discrete Multi-Physics for studying the dynamics of emboli in flexible venous valves

M. Ariane[a,*], D. Vigolo[a], A. Brill[b], F. G. B Nash[b], M. Barigou[a], A. Alexiadis[a,*]

[a] School of Chemical Engineering, University of Birmingham, Birmingham, United Kingdom

[b] Institute of Cardiovascular Sciences, University of Birmingham, Birmingham, United Kingdom

## Abstract

Emboli, which are parts of blood clots, can be stuck in the vasculature of various organs (most frequently, lungs) and cause their malfunction or even death. In this work, using mathematical modelling, different types of emboli-like structures are studied in a double venous valve system. The model is implemented with a fully Lagrangian Discrete Multi-Physics technique and the flow is governed by flexible walls. The study shows the effect of different diameters and lengths of a free embolus in the flow surrounding the valve. The presence of an embolus strongly affects the dynamics of both the fluid and the leaflets in venous valves and the permanence of the embolus in the valve chamber is narrowly linked with its length.

**Keywords:** Discrete Multi-Physics, Smoothed Particle Hydrodynamics, Mass and Spring Model, biological venous valve, Emboli, Deep Venous Thrombosis.

# 1. Introduction

An embolus is generally formed when a section of a thrombus detaches and circulates in the cardiovascular system until reaching narrow vessels, most frequently, in the lungs [1-3]. When emboli are trapped, they can obstruct blood flow in the lungs leading to a potentially life-threatening complication known as pulmonary embolism (PE) or deep vein thrombosis (DVT). In the UK alone, around 25,000 deaths are caused by PE or DVT; this number is five times higher than those from breast cancer, AIDS and road accidents combined [4].

While medical research highlights the role of DVT on the hydrodynamics around venous valves [5], the actual physical interaction of the embolus with the valve remains unexplored. The literature provides a wide range of publications about venous and arterial thrombosis, but the majority of these studies focuses on thrombogenesis and clotting [6-14], rather than the dynamics of the embolus.

To circumvent the current limitations of in-vivo and in-vitro models, computer simulations (in-silico modelling) of the the venous valve have been carried out but, with a few exceptions [13, 15, 16], emboli are not accounted for. For DVT however, this represents a serious limitation since the presence of the embolus changes considerably the hydrodynamics around the valve.

Previous studies [15, 16] have shown that the diameter, the elasticity and the location of an embolus affect the flow in arterial bifurcations [15] or in Inferior Vena Cava (IVC) [16]. But the interaction of the embolus with more complex settings such as the flexible leaflets of the venous valve has not been investigated. Only Simão et Al. [13] consider the presence of solid

41 particles in the venous valve, but these are simple Lagrangian point particles and the flow,
42 therefore, is not fully resolved around them.

43 By modelling the physical interaction of emboli with different shapes and flexibilities with
44 the soft leaflets of the venous valve and the change of hydrodynamics that this involves, this
45 paper fills a gap in the literature since the valve environment is probably the most critical for
46 DVT and the presence of clots in the vicinity of the valve has been associated with the
47 occurrence of new thrombosis activation sites [5].

# 2. Methodology

## 2.1. Modelling

A hybrid approach, based on a particle framework, is implemented to model haemodynamics and solid structure deformation. The technique, called Discrete Multi-Physics (DMP) [14, 17, 18], associates Smoothed Particle Hydrodynamics (SPH) [19-21] and the Mass and Spring Model (MSM) [22-24] and has been used to model the fluid-structure interactions occurring in deep vein valves [14], cardiac valves [17] and the intestine [18].

In this approach, the liquid is represented by SPH particles that interact with each other by viscous and pressure forces and the tissues by MSM particles inter-connected by means of computational springs (to model the elastic modulus) and dashpots (to model viscoelasticity). The essential ideas behind the DMP method are summarized in Appendix A; the reader can refer to [24] for a more extensive explanation of the DMP theory and to [22] for applications in different fields such as lava flows, cell dynamics and solid-liquid flow.

## 2.2. Geometry

In this study, we use a 2D schematic representation of a double leg venous valve system. The geometry is similar to the short valve model [14] but here it is used with two antagonist valves (Fig. 1). The channel radius is $Z$ = 0.004 m, the membrane length is $L$ = 0.01m, the radius of the valve chamber is $R$ = 0.007 m and its length is $Y$ = 0.04 m [14]. The two valve systems are inter-connected and the total length between the two chambers is $C$ = 0.048 m (0.046 m in [25]). The external walls are divided into four parts: two flexible sections where an external force is applied (Channel 1 and Channel 2 in Fig. 1), and two valve chambers

(Valve chamber 1 and Valve chamber 2 in Fig. 1) that contain the leaflets. Since periodic boundary conditions are enforced, the fluid exiting from the channel opening on the right is reinserted to the channel opening on the left and vice versa. For the same reason, Channel 1 in Fig. 1 appears to be divided into two sections (one on the left and another on the right), but, computationally, the two ends are joined together by the periodic boundary conditions. A net fluid flow is achieved by means of external forces acting alternatively on Channel 1 and Channel 2 (Fig. 1). When a 'squeezing' force *F* (see Fig. 1) is applied to Channel 1, Valve 1 opens, Valve 2 closes, and the fluid flows from the left to the right. When *F* is applied to Channel 2, Valve 2 opens, Valve 1 closes, and the fluid maintains the same direction from the left to the right. This approach mimics the actual motion of blood in the legs' veins induced by the contraction of the surrounding muscles.

In the rest of the paper, we refer to the regions between the leaflets (in both Valve 1 and Valve 2) as the 'opening regions' and to the regions between the walls and the leaflets (in both Valve chamber 1 and Valve chamber 2) as 'sinus regions' (Fig. 1).

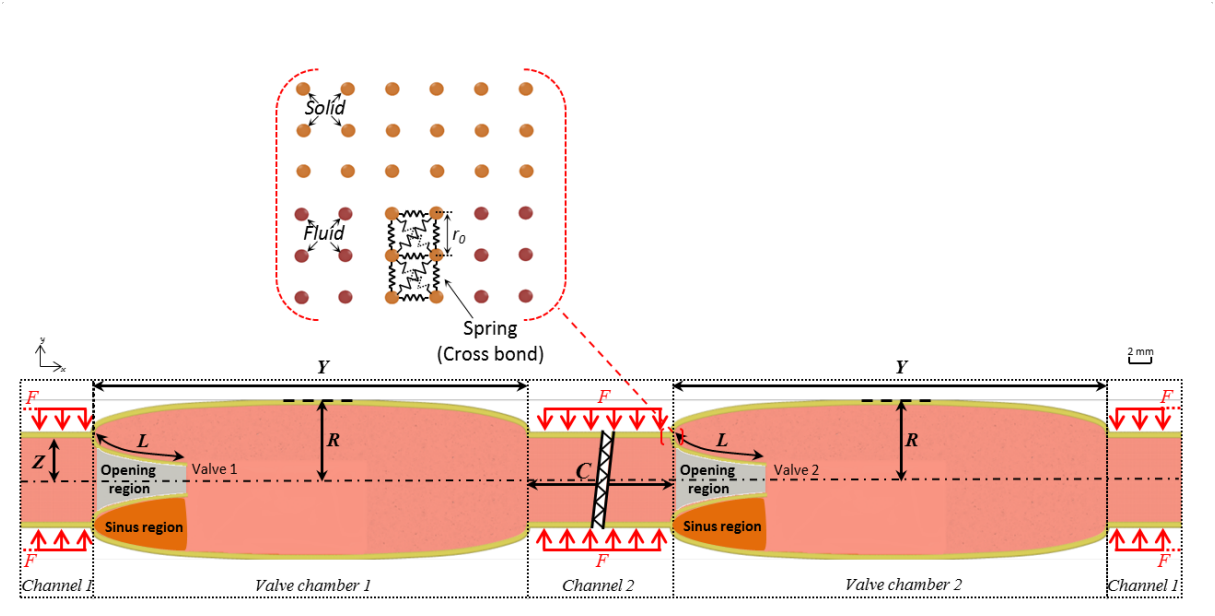

Fig. 1. Illustration of the double venous valve 2D geometry.

According to the DMP approach (see Appendix A) both the fluid and the solid are represented by discrete computational entities, which we call ‘fluid particles’ and ‘solid particles’. The different behaviour of fluid and solid particles depends on the type of forces the DMP algorithm applies to each computational particle. If these forces model the viscous and pressure forces commonly acting on fluids, the computational particle behaves like a fluid; if they model the viscoelastic forces acting on solid, the particle behaves like a solid. Computationally, the fluid forces are calculated with the SPH method while the solid forces particles by means of springs (MSM model) as detailed in Appendix A. The wall delimiting the valve chamber is considered stationary and, therefore, no forces are applied to the computational particle representing this part of the domain. Solid-liquid boundary conditions are also modelled by means of inter-particle forces that model no-penetration and no-slip conditions as explained in Appendix A.

## 2.3. Model parameters

In our simulations, the geometry is divided into 168676 particles spaced of $10^{-4}$ m: 584 for the valves, 10722 for the walls, and 157370 for the fluid area. As mentioned, SPH particles are used for the fluid, stationary (solid) particles for the valve chamber walls and MSM particles for the flexible walls and the leaflets. Three layers of particles are used for the walls and two for each leaflet, with thicknesses of $3.10^{-4}$ m and $2.10^{-4}$ m, respectively. The flow is laminar [13, 25, 26] and blood is here considered a Newtonian fluid [15, 27]. Table 1 gathers all the parameters used in the simulation.

Table 1. Model parameters used in the simulations.

| SPH (Eqs. A.5−A.7) | |
|---|---|
| **Parameter** | **Value** |
| Number of SPH wall particles (3 layers) | 10722 |
| Number of SPH valve particles (2 layers) | 584 (146 particles/leaflet) |
| Number of SPH fluid particles | 157370 |
| Mass of each particle (fluid) | $1.05 \cdot 10^{-5}$ kg |
| Mass of each particle (solid) | $2 \cdot 10^{-5}$ kg |
| Initial distance among particles $\Delta r$ | $1 \cdot 10^{-4}$ m |
| Smoothing length $h$ | $2.5 \cdot 10^{-4}$ m |
| Artificial sound speed $c_0$ | 10 m $s^{-1}$ |
| Density $\rho_0$ | 1056 kg $m^{-3}$ |
| Viscosity $\mu_0$ | 0.0035 Pa s |
| Time step $\Delta t$ | $10^{-6}$ s |
| Force $F$ | 0.008 N |
| MSM (Eqs. A.10) | |
| **Parameter** | **Value** |
| Hookian coefficient $k_b$ (Wall) | $1 \cdot 10^{5}$ J $m^{-2}$ |
| Hookian coefficient $k_b$ (membrane) | $5 \cdot 10^{6}$ J $m^{-2}$ |
| Viscous damping coefficient $k_v$ (Wall) | 1 kg $s^{-1}$ |
| Viscous damping coefficient $k_v$ (membrane) | 0.1 kg $s^{-1}$ |
| Equilibrium distance $r_0$ | $1 \cdot 10^{-4}$ m |
| BOUNDARIES (eq. A.14) | |
| Constant $K$ | $4 \cdot 10^{-4}$ J |
| Repulsive radius $r^*$ | $1 \cdot 10^{-4}$ m |

## 2.4. Simulation parameters

As detailed in Appendix A, the structure of the flexible tissue (wall and valve) and its elasticity are implemented with a spring model. The spring constant $k_b$ has been chosen in order to model the different elastic properties of the leaflets and the walls (Table 1). A viscous coefficient ($k_v$) is also added to the MSM springs to confer viscoelastic properties to the valve and the flexible wall as in a Kelvin–Voigt material.

The inlet/outlet of the fluid in the *x*-direction is controlled using periodic boundary conditions. The flow is pulsed periodically and generates several opening and closing of the valves. Therefore, we use the term “cycle” to define a single period including one opening and one closing of the same valve [25, 26]. For each cycle, we model the opening phase by applying a vertical force *F* (Y-axis) on Channel 2 for 1.5 s while no force is applied to Channel 1 (Fig. 1). During the closing phase (1.5 s), Channel 2 is relaxed (*F* on Channel 2 is set to 0) and *F* is applied to Channel 1. The force *F* is constant and uniform for each cycle (Table 1). For all simulations, a total of 10 cycles (30 s) are calculated.

## 2.5. Emboli

A solid, embolus-like structure is introduced into the flow. The solid particles of the embolus are joined together by springs whose Hook constant is reported in Table 2. Differently from some of our previous studies [14, 17] where the embolus grows due to an aggregation algorithm, here the embolus size is fixed during the simulation.

The effect of size, length and embolus’ flexibility is investigated (Table 2). In the literature, no standard size or length for emboli is given and the shape mostly depends on the surrounding flow, channel diameter and valve characteristics [13]. In this work, to account for a variety of potential cases, the selected sizes are in the range used by [16] and the lengths coincide with the length of (i) the sinus region (embolus L6 in Table 2), (ii) half of the valve chamber (embolus L19), (iii) the valve chamber (embolus L37) and (iv) the valve chamber + half of the channel (embolus L77).

136

137 Table 2. Simulation parameters used for the embolus aggregate.

| **Variation of the diameter of the embolus (spherical) with $k_b$ = 1 $10^4$ J $m^{-2}$** | | |
|---|---|---|
| Diameter of the embolus [m] | Location at t = 0 s | Case |
| 2.6 $10^{-3}$ m | Centre of the tube | D26 |
| 5.2 $10^{-3}$ m | Centre of the tube | D52 |
| 7.8 $10^{-3}$ m | Centre of the tube | D78 |
| **Variation of the length of the embolus with height = 2.6 $10^{-3}$ m and $k_b$ = 1·$10^4$ J $m^{-2}$** | | |
| Length of the embolus [m] | Location at t = 0 s | Case |
| 5.9 $10^{-3}$ m | Sinus region | L6 |
| 19 $10^{-3}$ m | Sinus region | L19 |
| 21 $10^{-3}$ m | Centre of the tube | L21 |
| 37 $10^{-3}$ m | Sinus region | L37 |
| 77 $10^{-3}$ m | Sinus region | L77 |
| **Variation of the flexibility of the embolus (spherical) with diameter = 7.8 $10^{-3}$ m** | | |
| Bond coefficient $k_b$ [J $m^{-2}$] | Location at t = 0s | Case |
| 1·$10^3$ J $m^{-2}$ | Centre of the tube | F103 |

138 # 3. Results and discussion

139 ## 3.1. Hydrodynamics

140 A typical simulation without the embolus is shown in Fig. 2. During the opening phase (of
141 Valve 1), when *F* is applied to Channel 1, the pressure in Channel 1 increases; Valve 1 opens
142 and Valve 2 closes (Fig. 2a and Fig. 2b). Part of the fluid leaves Channel 1 and accumulates
143 in Channel 2, which dilates. During the closing phase (of Valve 1), the force *F* is applied to
144 Channel 2 and Channel 1 relaxes (*F* is set to 0). Valve 1 closes while Valve 2 opens (Fig. 2c

and Fig. 2d). The contraction and, therefore, the force applied to the vein walls accounts for the level of physical activity of a specific individual. The force used in this study generates a peak blood velocity around 0.035 m $s^{-1}$ which corresponds to a low level of physical activity [13, 14]. This condition was chosen since the risk of DVT increases when the level of physical activity is low.

The valve opening-closing mechanism in relation to the contraction of the veins around the valve is confirmed by the available literature [14, 25, 26]. At the time of maximal contraction, however, the vein assumes an asymmetrical shape shown in Fig. 2d. This is probably due to the fact that, in our model, the segments of veins (Channel 1 and Channel 2) connecting two valves are considerably shorter than in reality. The asymmetrical shape can neither be confirmed nor disproved by available visualization data. This circumstance, however, has little relevance to our work, which focuses on the dynamics of the valves rather than that of the veins.

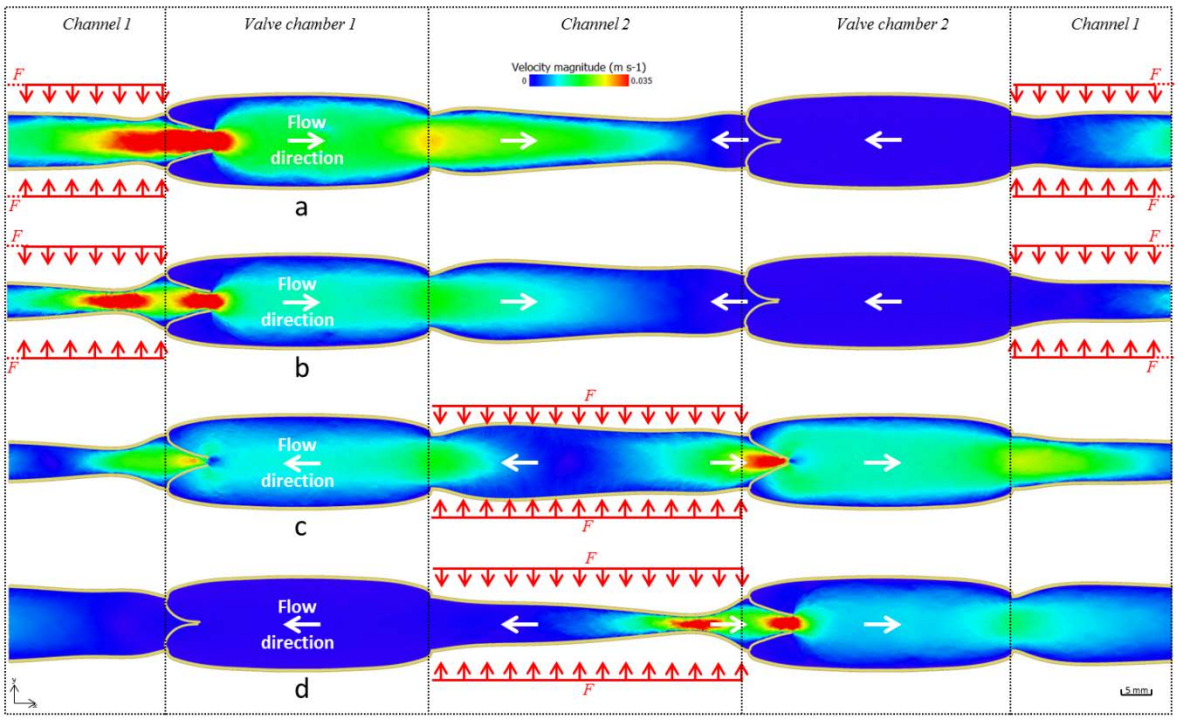


159

160 Fig. 2. Valve deformation and velocity magnitude of the system during a cycle: (a) t = 0 s, (b)

161 t = 0.75 s, (c) t = 1.5 s, (d) t = 2.25 s, (e) t = 3 s.

162 In the next section, we introduce an embolus-like structure both in the main flow (opening

163 region in Fig. 1) and behind the valve (sinus region in Fig. 1). The goal is to show how the

164 presence of a free embolus impacts the flow in the vicinity of the valve.

165 As mentioned, three parameters are investigated in this case: size, length and flexibility of the

166 aggregate (Table 2).

## 167 3.2. Embolus displacement in the opening region

168 Initially, three circular emboli with diameters of 2.6 $10^{-3}$ m (Case D26 in Table 2), 5.2 $10^{-3}$ m

169 (D52) and 7.8 $10^{-3}$ m (D78) are introduced into the flow (Fig. 3a). In the first case (Fig. 3b),

170 the embolus is too small for impacting the flow and crosses the valve with no contact with the

171 leaflets. No significant difference with the pure fluid case is observed.

In the second case (Fig. 3c), although the embolus diameter is bigger than the valve opening, it can cross the valve because of its flexibility and the deformation of the leaflets. The embolus is elastic [15] and recovers its initial shape after the valve. However, contrary to the first case, the flow surrounding the embolus is considerably affected by the presence of the embolus and two vortexes form around the valve.

In the third case (Fig. 3d), the embolus is bigger than the inlet valve chamber and despite the large deformation of both the embolus and the valve, the embolus cannot cross the valve.

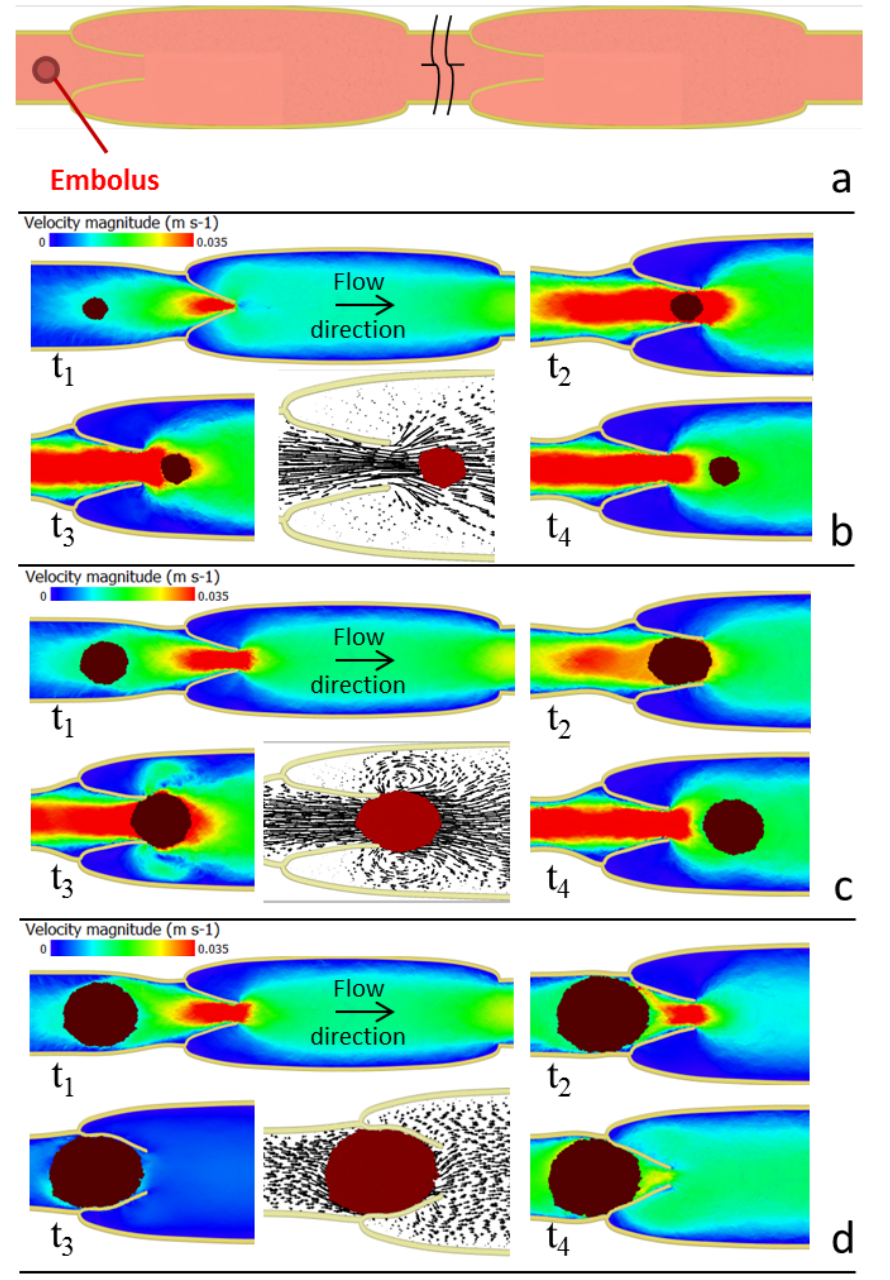


179

180 Fig. 3. Embolus position and velocity vectors at different times: a) t = 0 s for all emboli, b)

181 embolus D26, c) embolus D52, and d) embolus D78.

182 In reality, the embolus obstruction observed in Fig. 3d would probably resolve itself after a

183 certain time since, normally, the level of physical activity of an individual changes during the

184 day [28], while in our simulation we only considered low physical activity. In our

185 simulations, a similar situation (i.e. an embolus, initially stuck, crosses the valve after several
186 cycles) occurs when the flexibility of the embolus is higher (Fig. 4).

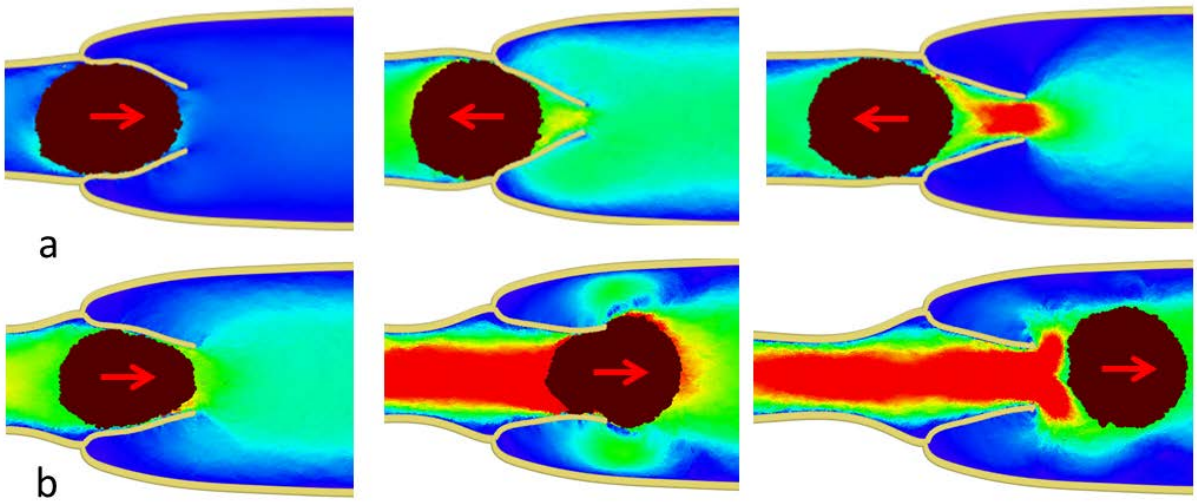


187

188 Fig. 4. Embolus of diameter 7.8 $10^{-3}$ m with different elasticity: a) kb = 1 $10^{4}$ J $m^{-2}$ (D78) and
189 b) kb = 1 $10^{3}$ J $m^{-2}$ (F103).

190 The vortexes observed in Fig. 3c and Fig. 4 are larger if the length of the embolus is longer as
191 in Fig. 5. In this case, both the flow and the valve behaviour are considerably altered by the
192 presence of the ‘sausage-like’ embolus.

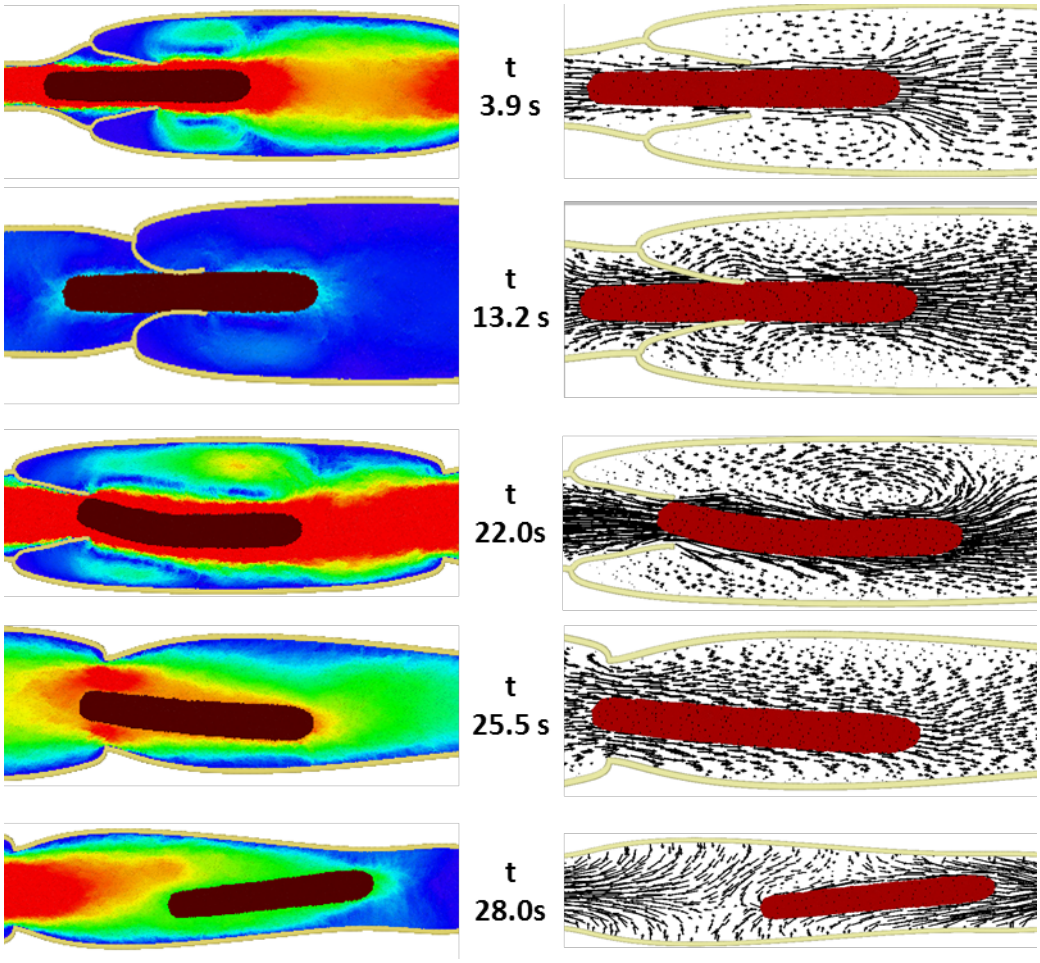


Fig. 5. Velocity magnitude and vectors of the flow and circulation of the embolus (L21) at different times.

## 3.3. Embolus displacement in the sinus region

In this section, an embolus is located behind Valve 1 (sinus region in Fig. 1). In the medical literature, it is not completely clear where emboli form, but they are often found in the sinus region. After they reach a certain size, they leave the sinus region, and move in the cardiovascular system. In this section, we show how the length of the embolus can affect its permanence in the sinus region. Four emboli with different lengths are simulated (Table 2):

5.9 mm (L6 in Table 2), 19 mm (L19), 37 mm (L37) and 77 mm (L77) and located in the sinus region (Fig. 6a).

Fig. 6b and Fig. 6c show no significant displacement of embolus L6 and embolus L19 after 10 cycles while embolus L37 (Fig. 6d) and L77 (Fig. 6e) show a high displacement. In fact, each embolus interacts with the fluid in a different way. The longer the embolus, the higher the drag force that the liquid exchange with the embolus. This force, however, is not simply proportional to its length, but it also depends on the local velocity at the location of the embolus.

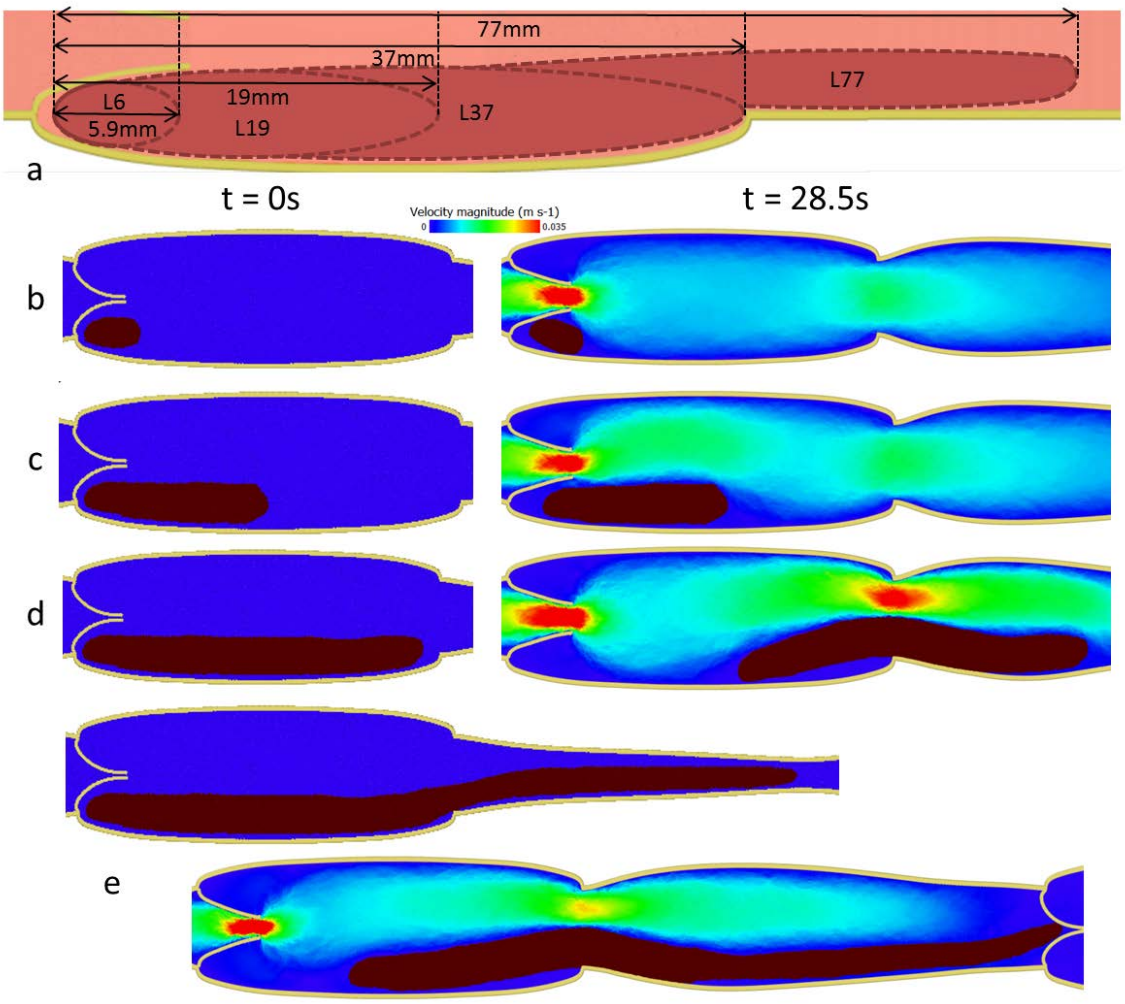


Fig. 6. Embolus position at t = 0 s and t = 28.5 s for a) L6, b) L19, c) L37, d) L77.

In Fig. 7, embolus displacement versus the simulation time indicates that the displacement values oscillate every cycle (forward and backward embolus motion). Embolus L6 never moves and only spins around itself (Fig. 6b) due to its “circular” shape. While embolus L19 begins to move slowly after 20 s. In both cases, the emboli remain in the low flow area (Fig. 8) where the flow velocities are the lowest. On the other extreme, embolus L77 continually moves because the most of the embolus is located in the main flow area (Fig. 8). The displacement of L37 is initially smaller than L77, because a lower fraction is in contact with the high velocity area. However, once it is dragged away from the left end of the sinus it is more easily captured by the main flow due to its smaller size.

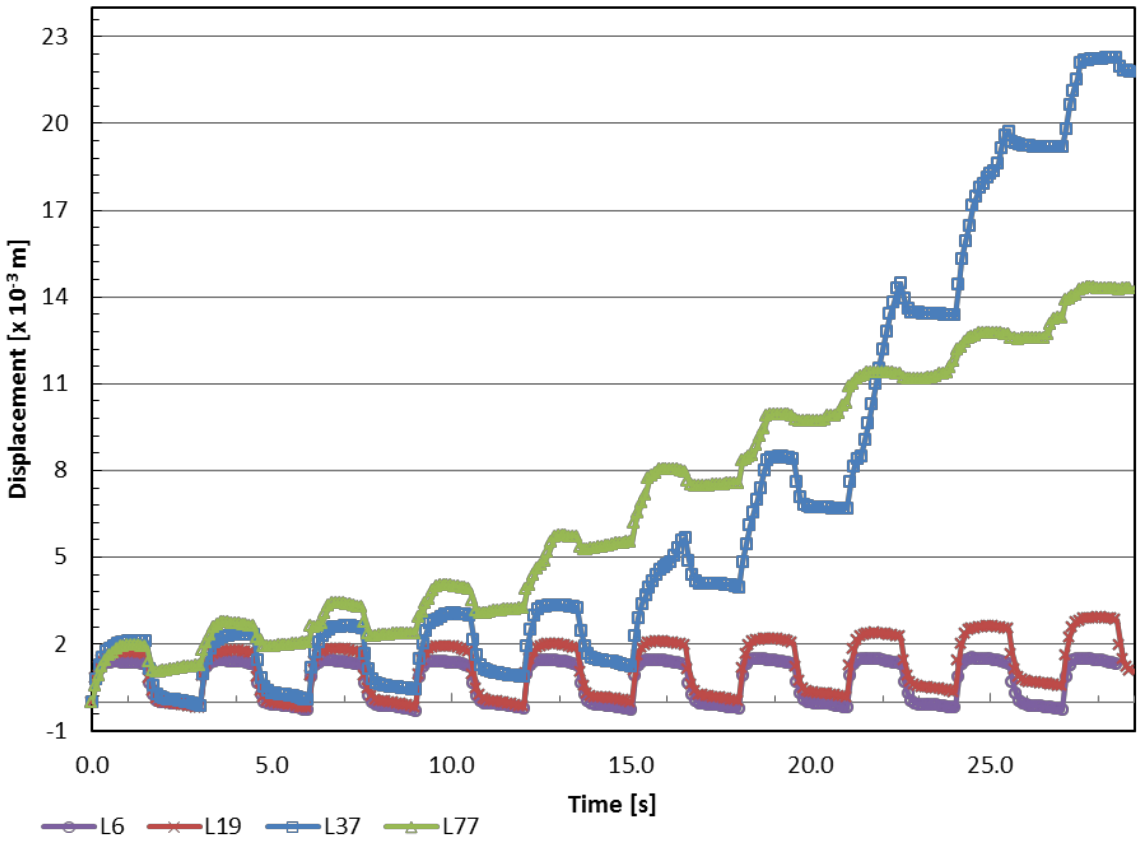


Fig. 7. Time evolution of the local displacement for embolus L6, L19, L37, and L77.

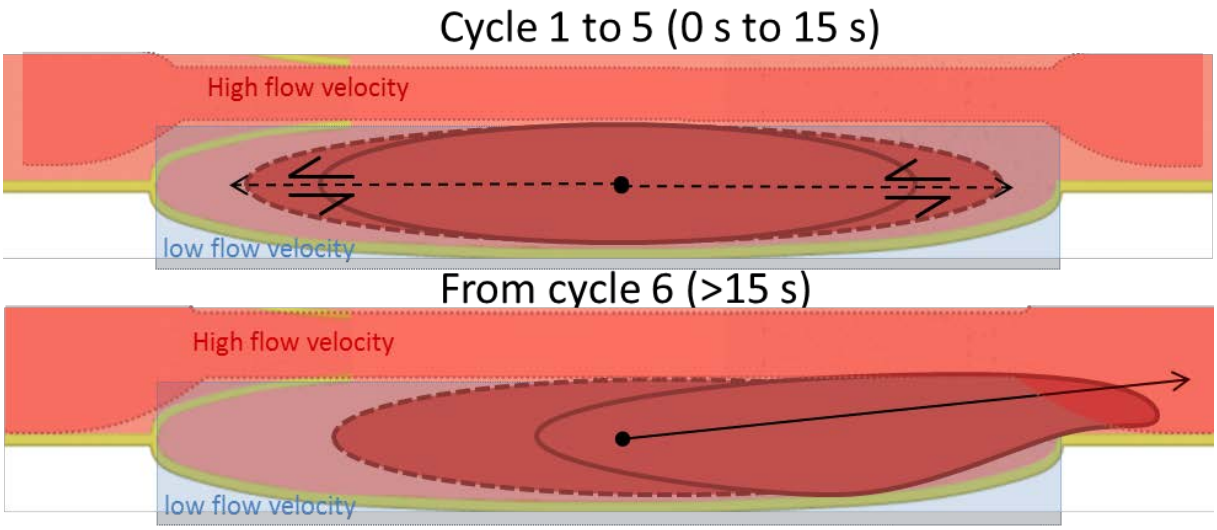


Fig. 8. Schematic of embolus L37 movement in low flow region and high flow region before and after 15s.

# 4. Conclusions

Free emboli circulation in a valve environment has been studied using the Discrete Multi-Physics approach. We modelled both fluid and emboli dynamics as well as the leaflets deformation. In our previous studies [14, 17], an inlet fluid velocity was used to ensure the blood motion within the rigid channel, while here, the flow is governed by muscle contractions.

The results show that emboli with a size bigger than the valve can still cross the valve if they are flexible enough. This observation can be linked with the age of emboli in the body since the elasticity of an embolus depends on its life-time in the blood system [29], and the older the embolus the lower its flexibility.

The embolus length plays also a paramount role. In the main flow (opening region), the embolus can potentially generate new vortex area that can further favour platelets

aggregation. In the low flow (sinus region), the length of the embolus determines how long it takes for the embolus to detach from the sinus region and move within the main flow.

The main conclusion of this work is that the presence of an embolus strongly affects the dynamics of both the fluid and the leaflets in venous valves. Therefore, computer simulations designed to support fundamental research in DVT should account for emboli if they aim at a more realistic description of reality.

# Supporting Information

Appendix A

# References


[1] MacIver DH, Adeniran I, MacIver IR, Revell A, Zhang HG. Physiological mechanisms of pulmonary hypertension. American Heart Journal. 2016;180:1-11.

[2] Reitsma PH, Versteeg HH, Middeldorp S. Mechanistic View of Risk Factors for Venous Thromboembolism. Arteriosclerosis Thrombosis and Vascular Biology. 2012;32:563-8.

[3] Tapson VF. Acute Pulmonary Embolism. The New England journal of medecine. 2008:1037-52.

[4] Hunt BJ. The prevention of hospital-acquired venous thromboembolism in the United Kingdom. British Journal of Haematology. 2009;144:642-52.

[5] Esmon CT. Basic mechanisms and pathogenesis of venous thrombosis. Blood Reviews. 2009;23:225-9.

[6] Narracott A, Smith S, Lawford P, Liu H, Himeno R, Wilkinson I, et al. Development and validation of models for the investigation of blood clotting in idealized stenoses and cerebral aneurysms. Journal of Artificial Organs. 2005;8:56-62.

[7] Zhang J-n, Bergeron AL, Yu Q, Sun C, McIntire LV, López JA, et al. Platelet Aggregation and Activation under Complex Patterns of Shear Stress. Thrombosis and Haemostasis. 2002;88:817-21.

[8] Harrison SE, Bernsdorf J, Hose DR, Lawford PV. A lattice Boltzmann framework for simulation of thrombogenesis. Progress in Computational Fluid Dynamics. 2008;8:121-8.

[9] Carrascal PG, Garcia JG, Pallares JS, Ruiz FC, Martin FJM. Numerical Study of Blood Clots Influence on the Flow Pattern and Platelet Activation on a Stented Bifurcation Model. Ann Biomed Eng. 2017;45:1279-91.

[10] Hou XY, Sun X, Shi YT, Zhang KL, Yao JT. Simulation of the Formation Mechanism of Coronary Thrombosis Based on DEM-CFD Coupling. 2015 8th International Conference on Biomedical Engineering and Informatics (Bmei). 2015:24-8.

[11] Ouared R, Chopard B. Lattice Boltzmann simulations of blood flow: Non-Newtonian rheology and clotting processes. Journal of Statistical Physics. 2005;121:209-21.

[12] Diamond SL. Systems Analysis of Thrombus Formation. CircRes. 2016;118:1348-62.

[13] Simão M, Ferreira JM, Mora-Rodriguez J, Ramos HM. Identification of DVT diseases using numerical simulations. Medical & Biological Engineering & Computing. 2016;54:1591-609.

[14] Ariane M, Wen W, Vigolo D, Brill A, Nash FGB, Barigou M, et al. Modelling and simulation of flow and agglomeration in deep veins valves using discrete multi physics. Computers in Biology and Medicine. 2017.

[15] Abolfazli E, Fatouraee N, Vahidi B. Dynamics of motion of a clot through an arterial bifurcation: a finite element analysis. Fluid Dynamics Research. 2014;46.

[16] Aycock KI, Campbell RL, Manning KB, Craven BA. A resolved two-way coupled CFD/6-DOF approach for predicting embolus transport and the embolus-trapping efficiency of IVC filters. Biomechanics and Modeling in Mechanobiology. 2017;16:851-69.

[17] Ariane M, Allouche MH, Bussone M, Giacosa F, Bernard F, Barigou M, et al. Discrete multi-physics: A mesh-free model of blood flow in flexible biological valve including solid aggregate formation. Plos One. 2017;12.

[18] Alexiadis A, Stamatopoulos K, Wen W, Batchelor HK, Bakalis S, Barigou M, et al. Using discrete multi-physics for detailed exploration of hydrodynamics in an in vitro colon system. Computers in Biology and Medicine. 2017;81:188-98.

[19] Monaghan JJ. Simulating Free Surface Flows with SPH. Journal of Computational Physics. 1994;110:399-406.

[20] Morris JP, Fox PJ, Zhu Y. Modeling Low Reynolds Number Incompressible Flows Using SPH. Journal of Computational Physics. 1997;136:214-26.

[21] Liu GR, Liu MB. Smoothed Particle Hyrodynamics: a meshfree method. In: Ltd WSPCP, editor. World Scientific Publishing Co. Pte. Ltd ed. Singapore: World Scientific Publishing Co. Pte. Ltd; 2003. p. 473.

[22] Alexiadis A. The Discrete Multi-Hybrid System for the Simulation of Solid-Liquid Flows. Plos One. 2015;10.

[23] Alexiadis A. A new framework for modelling the dynamics and the breakage of capsules, vesicles and cells in fluid flow. In: BarthesBiesel D, Blyth MG, Salsac AV, editors. Iutam Symposium on Dynamics of Capsules, Vesicles and Cells in Flow2015. p. 80-8.

[24] Alexiadis A. A smoothed particle hydrodynamics and coarse-grained molecular dynamics hybrid technique for modelling elastic particles and breakable capsules under various flow conditions. International Journal for Numerical Methods in Engineering. 2014;100:713-9.

[25] Wijeratne NS, Hoo KA. Numerical studies on the hemodynamics in the human vein and venous valve. 2008 American Control Conference, Vols 1-12. New York: Ieee; 2008. p. 147-52.

[26] Lurie F, Kistner RL, Eklof B, Kessler D. Mechanism of venous valve closure and role of the valve in circulation: a new concept. Journal of Vascular Surgery. 2003;38:955-61.

[27] Thomas B, Sumam KS. Blood Flow in Human Arterial System-A Review. Procedia Technology. 2016;24:339-46.

[28] Collins R, Scrimgeour A, Yusuf S, Peto R. Reduction in fatal pulmonary embolism and venous thrombosis by perioperative administration of subcutaneous heparin. Overview of

results of randomized trials in general, orthopedic, and urologic surgery. The New England journal of medicine. 1988;318:1162-73.

[29] Chueh JY, Wakhloo AK, Hendricks GH, Silva CF, Weaver JP, Gounis MJ. Mechanical Characterization of Thromboemboli in Acute Ischemic Stroke and Laboratory Embolus Analogs. American Journal of Neuroradiology. 2011;32:1237-44.